CNR is gratefully acknowledged.

References and Notes

(1) Natta, G.; Pino, P.; Mazzanti, G.; Corradini, P.; Giannini, U. *Rend. Acc. Naz. Lincei (VIII)* **1955**, *19*, 397. Such polymerization has been called "stereoselective" by Natta and Pino.
(2) Pino, P.; Ciardelli, F.; Montagnoli, G. *J. Polym. Sci., Part C* **1969**, *16*, 3256.
(3) Ciardelli, F.; Locatelli, P.; Marchetti, M.; Zambelli, A. *Makromol. Chem.* **1974**, *175*, 923.
(4) Pino, P. *Adv. Polym. Sci.* **1965**, *4*, 393.
(5) (a) Zambelli, A. *NMR Basic Princ. Prog.* **1971**, *4*, 101. (b) Zambelli, A.; Gatti, G.; Sacchi, M. C.; Crain, W. O.; Roberts, J. D. *Macromolecules* **1971**, *4*, 475. In this paper the word enantioselective is always related to carbon 2 (enantiotopic) of the monomer, which becomes chiral after the insertion. The word diastereoselective is used with reference to the different reactivity of the diastereotopic faces of the monomer toward the insertion.
(6) Shelden, R. A.; Fueno, T.; Tsunetsugu, T.; Furokawa, J. *J. Polym. Sci., Part B* **1965**, *3*, 23.
(7) (a) Zambelli, A.; Sacchi, M. C.; Locatelli, P.; Zannoni, G. *Macromolecules* **1982**, *15*, 211. (b) Zambelli, A.; Locatelli, P.; Sacchi, M. C.; Tritto, I. *Macromolecules* **1982**, *15*, 831.
(8) Wolfsgruber, C.; Zannoni, G.; Rigamonti, E.; Zambelli, A. *Makromol. Chem.* **1975**, *176*, 2765.
(9) Stereochemical notation proposed by: Frisch, H. L.; Malllows, C. L.; Bovey, F. A. *J. Chem. Phys.* **1966**, *45*, 1565.
(10) Grant, D. M.; Paul, E. G. *J. Am. Chem. Soc.* **1964**, *86*, 2984.
(11) The configurational notation is that of: Cahn, R. S.; Ingold, C. R.; Prelog, V. *Angew. Chem., Int. Ed. Engl.* **1956**, *5*, 365.
(12) Eight more stereochemical environments are possible. Since they are mirror images of the ones considered, they are omitted.
(13) As reported in a previous paper,[14] the vicinal methyl carbons lying on the same side of the Fisher projection are defined as erythro (e) and those lying on the opposite side are defined as threo.
(14) Zambelli, A.; Gatti, G. *Macromolecules* **1978**, *11*, 485.
(15) Lazzaroni, R.; Salvadori, P.; Bertucci, C.; Veracini, C. A. *J. Organomet. Chem.* **1976**, *99*, 475.
(16) Lazzaroni, R.; Salvadori, P.; Pino, P. *J. Organomet. Chem.* **1972**, *43*, 233.
(17) Unpublished results from our laboratory.
(18) The molecular weight of the polymer is very low due to the presence of $Zn(CH_3)_2$, which is an effective chain-transfer agent. The solubility of the polymer arises from the low molecular weight of the fraction (see Table II) and not from lack of stereoregularity. See, e.g.: Natta, G.; Giacchetti, E.; Pasquon, I.; Pajaro, G. *Chim. Ind. (Milan)* **1960**, *42*, 1091.
(19) Nozakura, S.; Takeuchi, S.; Yuki, H.; Murahashi, S. *Bull. Chem. Soc. Jpn.* **1961**, *34*, 1673.
(20) Petraccone, V.; Ganis, P.; Corradini, P.; Montagnoli, G. *Eur. Polym. J.* **1972**, *8*, 99.
(21) $C^*_{R'}$ are the chiral active sites preferring during the propagation (or even in the initiation if the alkyl group bonded to the active metal is primary and larger than CH_3) the addition of the monomer (either *R* or *S*) to give a backbone substituted carbon of *R'* configuration. On the $C^*_{S'}$ sites the mirror image steps occur, giving mirror image end groups. The configuration of the backbone substituted carbons is assigned as reported in the caption of Figure 4, i.e., neglecting the isotopic substitution and assuming that the left side of the growing chain has a higher rank since the active metal of the catalytic sites is assumed to be at the left side of the chain. A consequence of this convention is that the attack on the *R'* (or *S'*) face of the monomer gives *S'* (or *R'*) (see Figure 2) backbone substituted carbons. In the equations of Scheme I are reported the configurational notations of the monomer units. The configuration of the backbone carbons is primed. The drawing of the stereochemical environment of the end groups is reported in Figure 1 under the corresponding labeling (AI, etc.). The A-labeled end groups have the enriched $^{13}CH_3$ in an erythro relationship with the CH_3 of the substituent of the first inserted monomer unit and the B-labeled end groups have the $^{13}CH_3$ in a threo relationship.
(22) It is assumed that the propagation rate constants are the same as those reported in Schemes I and II for the insertion of the second monomer unit.
(23) No fraction showed $I_{BI}/I_{BIV} < 1$. Most probably this is due to the fact that the lowest molecular weight fraction (oligomer) is lost because of the solubility in methanol.
(24) Zambelli, A.; Locatelli, P.; Rigamonti, E. *Macromolecules* **1979**, *12*, 156.
(25) The equation is referred to the propagation steps on the *R'*-preferring sites. For symmetry the diastereoselectivity on the *S'*-preferring sites is the same:

$$\frac{k_{R'(R'S)(R'S)} + k_{R'(R'R)(R'S)}}{k_{R'(R'R)(R'R)} + k_{R'(R'S)(R'R)}} = \frac{k_{S'(S'R)} + k_{S'(S'S)(S'R)}}{k_{S'(S'S)(S'S)} + k_{S'(S'R)(S'S)}}$$

(26) Greenwald, H.; Chaykovsky, M.; Corey, E. J. *J. Org. Chem.* **1963**, *28*, 1128.
(27) Pino, P.; Lardicci, L.; Centoni, C. *J. Org. Chem.* **1959**, *24*, 1399.
(28) Natta, G.; Morandi, M.; Crespi, G.; Moraglio, G. *Chim. Ind. (Milan)* **1957**, *39*, 275.

A Computer Model for the Gel Effect in Free-Radical Polymerization

Wen Yen Chiu, Gregory M. Carratt, and David S. Soong*

Department of Chemical Engineering, University of California, Berkeley, Berkeley, California 94720. *Received July 1, 1982*

ABSTRACT: A mathematical model is developed to describe free-radical polymerization reactions exhibiting a strong gel effect. Diffusion limitation is viewed as an integral part of the chain termination process from the very beginning of polymerization. Its effect on the overall rate of termination gradually increases with conversion and becomes dominant around certain conversion levels traditionally associated with the onset of the gel effect. Influence of temperature, concentration, and molecular weight on the relative importance of reaction vs. diffusion is properly accounted for by the model. The model also considers the glass effect, which occurs only at very high conversions when even monomer diffusion to reactive radical sites is severely curtailed. Thus, the developed model describes the polymerization process over the entire course of reaction. Model predictions have been compared with literature data on conversion history and product molecular weights for isothermal poly(methyl methacrylate) polymerization.

Introduction

The two major sources of problems encountered in industrial liquid-phase polymerization processes are the heat released by the highly exothermic reactions and the great increase in viscosity of the reacting media over the course of polymerization. For a typical addition polymerization the heat of polymerization ranges from 10 to 20 kcal/mol, which can result in an adiabatic temperature rise of 200–400 °C. This large generation of heat, coupled with the low thermal diffusivity of the reacting mixture, often

0024-9297/83/2216-0348$01.50/0

leads to thermal runaway. Therefore, control of the process is difficult. A temperature rise generally lowers the degree of polymerization. Hence, large temperature variations in the course of the reaction broaden the product molecular weight distribution, with accompanying deterioration of mechanical properties of the polymer. The other serious problem occurring in most addition polymerizations is associated with the high viscosity of the system and the consequently low rate of diffusion-controlled termination. This is referred to as the Trommsdorff or gel effect.[1,2] The onset of the gel effect frequently causes uncontrollable reactions, resulting in excessive temperature rise, rapid conversion, and plugging of equipment.

The above discussion underlines the importance of a fundamental understanding of the various factors governing the reaction kinetics of polymerization, in particular, in the gel effect region. Only through basic knowledge about the molecular origins causing autoacceleration can improved process strategies be developed to combat the aforementioned problems effectively. Numerous attempts have thus been made to study and model chain polymerization to high conversions. A number of well-known models[3-8] have been developed, achieving differing degrees of success in fitting experimental data. Along with these modeling efforts, kinetic experiments have also been carried out in an attempt to determine the effects of concentration, viscosity, and molecular weight on the rate of polymerization.[9-12] Despite such extensive research, a consistent viewpoint on the underlying molecular processes controlling the rate of polymerization has not yet emerged. Furthermore, a convenient but quantitative model capable of describing free-radical polymerization over the entire course of reaction under both isothermal and nonisothermal conditions has not been fully established. It is especially desirable to develop such a mathematical model to predict the performance and outcome of a given polymerization process and to correlate the product specifications with various operating parameters such as reactor temperature history, initiator loading, and solvent concentration. This need prompted the present work, which examines the gel effect in light of the fundamental molecular processes governing the various steps of the termination reaction. In addition, the glass effect, which occurs only at very high conversions—when even monomer diffusion is severely curtailed—is considered. Thus, the developed model describes the polymerization process over the entire course of reaction.

Theory

1. Reaction Mechanism and Kinetic Equations. The objectives of this model development are multiple. In order for the model to be useful in process simulation and design calculation, it must quantitatively predict experimental data obtained under well-controlled conditions while requiring only a small number of adjustable parameters. Second, the model parameters preferably have a physical significance, so that their values can be reasonably estimated a priori for different systems. Finally, the mathematics must be easily implemented on a computer. The model developed in this work strives to reach these goals. It is designed to describe free-radical chain polymerization over the entire course of reaction, encompassing both the gel effect and glass effect regions. Predictions of this model are tested against conversion and molecular weight data from isothermal batch reactors.

The reaction mechanism adopted here consists of straightforward initiation, propagation, and termination. Chain-transfer reactions are neglected for convenience. The detailed mechanism is as follows:

Initiation

$$\mathrm{I} \xrightarrow{k_d} 2\mathrm{R}$$

$$\mathrm{R} + \mathrm{M} \xrightarrow{k_i} \mathrm{P}_1$$

Propagation

$$\mathrm{P}_n + \mathrm{M} \xrightarrow{k_p} \mathrm{P}_{n+1}$$

Termination

$$\mathrm{P}_n + \mathrm{P}_m \xrightarrow{k_{tc}} \mathrm{M}_{n+m}$$

$$\mathrm{P}_n + \mathrm{P}_m \xrightarrow{k_{td}} \mathrm{M}_n + \mathrm{M}_m$$

where I is the initiator, R is the primary initiator radical, M is the monomer, M_j is dead polymer with degree of polymerization j, P_j is the corresponding growing polymer radical, and the k's are the relevant rate constants.

For well-stirred batch reactions the following kinetic equations can be written. These primarily represent species balance for the initiator, monomer, and radicals

$$\frac{1}{V}\frac{\mathrm{d}(IV)}{\mathrm{d}t} = -k_d I \tag{1}$$

where V is the system volume,

$$\frac{1}{V}\frac{\mathrm{d}(MV)}{\mathrm{d}t} = -k_p MP \tag{2}$$

where $P = \sum_{n=1}^{\infty} P_n$,

$$\frac{1}{V}\frac{\mathrm{d}(RV)}{\mathrm{d}t} = 2fk_d I - k_i RM \tag{3}$$

where $0 \le f \le 1$ is an efficiency factor to account for other simultaneous processes consuming R,

$$\frac{1}{V}\frac{\mathrm{d}(P_1 V)}{\mathrm{d}t} = k_i RM - k_p MP_1 - k_t P_1 P \tag{4a}$$

$$\frac{1}{V}\frac{\mathrm{d}(P_n V)}{\mathrm{d}t} = k_p M(P_{n-1} - P_n) - k_t P_n P, \qquad n \ge 2 \tag{4b}$$

where $k_t \equiv k_{tc} + k_{td}$, and

$$\frac{1}{V}\frac{\mathrm{d}(M_n V)}{\mathrm{d}t} = k_{td} P_n P + \frac{1}{2}k_{tc}\sum_{m=1}^{n-1} P_m P_{n-m}, \qquad n \ge 2 \tag{5}$$

Fractional conversion is defined by $x \equiv (M_0V_0 - MV)/M_0V_0$ (M_0 and V_0 are the monomer concentration and the system volume, respectively, at $x = 0$), and volume contraction with conversion is considered by assuming that

$$V = V_0(1 + \epsilon x) \tag{6}$$

Here, ϵ is the volume expansion factor determined by $\epsilon \equiv (d_m - d_p)/d_p$, where d_m and d_p are the monomer and polymer density, respectively. Based on these definitions, we now have the following relationship between M and x:

$$M = M_0\frac{1 - x}{1 + \epsilon x} \tag{7}$$

In order to obtain average molecular weights of the growing radicals and resulting polymers, the method of moments is used. First, we define

$$\lambda_0 \equiv \sum_{n=1}^{\infty} P_n \tag{8a}$$

$$\lambda_1 \equiv \sum_{n=1}^{\infty} nP_n \tag{8b}$$

$$\lambda_2 \equiv \sum_{n=1}^{\infty} n^2 P_n \tag{8c}$$

or

$$\lambda_k \equiv \sum_{n=1}^{\infty} n^k P_n \tag{8d}$$

where λ_0, λ_1, and λ_2 are the zeroth, first, and second moment of the growing radicals, and

$$\mu_0 \equiv \sum_{n=1}^{\infty} M_n \tag{9a}$$

$$\mu_1 \equiv \sum_{n=1}^{\infty} nM_n \tag{9b}$$

$$\mu_2 \equiv \sum_{n=1}^{\infty} n^2 M_n \tag{9c}$$

or

$$\mu_k \equiv \sum_{n=1}^{\infty} n^k M_n \tag{9d}$$

where μ_0, μ_1, and μ_2 are the corresponding moments for the dead polymers.

The above defining equations and the linear volume contraction assumption can be substituted into the kinetic equations (eq 1–5) to give the following final equations for model calculation:

$$\frac{dI}{dt} = -k_d I - \frac{\epsilon I}{1+\epsilon x}\lambda_0(1-x)k_p \tag{10}$$

$$\frac{dx}{dt} = k_p(1-x)\lambda_0 \tag{11}$$

$$\frac{d\lambda_0}{dt} = -\frac{\epsilon\lambda_0^2}{1+\epsilon x}(1-x)k_p + 2fk_d I - k_t\lambda_0^2 \tag{12}$$

$$\frac{d\lambda_1}{dt} = -\frac{\epsilon\lambda_1\lambda_0}{1+\epsilon x}(1-x)k_p + 2fk_d I - k_t\lambda_0\lambda_1 + k_p\lambda_0 M_0\frac{1-x}{1+\epsilon x} \tag{13}$$

$$\frac{d\lambda_2}{dt} = -\frac{\epsilon\lambda_2\lambda_0}{1+\epsilon x}(1-x)k_p + 2fk_d I - k_t\lambda_0\lambda_2 + k_p M_0\frac{1-x}{1+\epsilon x}(2\lambda_1+\lambda_0) \tag{14}$$

$$\frac{d\mu_0}{dt} = -\frac{\epsilon\mu_0\lambda_0}{1+\epsilon x}(1-x)k_p + k_{td}\lambda_0^2 + \tfrac{1}{2}k_{tc}\lambda_0^2 \tag{15}$$

$$\frac{d\mu_1}{dt} = -\frac{\epsilon\mu_1\lambda_0}{1+\epsilon x}(1-x)k_p + k_{td}\lambda_0\lambda_1 + k_{tc}\lambda_0\lambda_1 \tag{16}$$

$$\frac{d\mu_2}{dt} = -\frac{\epsilon\mu_2\lambda_0}{1+\epsilon x}(1-x)k_p + k_{td}\lambda_0\lambda_2 + k_{tc}(\lambda_2\lambda_0 + \lambda_1^2) \tag{17}$$

Long-chain hypothesis is assumed in deriving the above equations. For the primary initiator free radical, R, the quasi-steady-state assumption ($V^{-1}\,d(RV)/dt = 0$) represents a reasonably accurate approximation. Hence, we have

$$k_i RM = 2fk_d I \tag{18}$$

Note that in this work, the above quasi-steady-state assumption is not extended to calculate the population of polymer radicals. We believe this assumption breaks down when the gel effect sets in, strongly impeding the termination process of these polymer radicals and causing a sudden surge in the radical population. As a result, eq 12–14 are included with the others in numerical integration to obtain model predictions. The initial conditions are $I = I_0$, and $x = \lambda_0 = \lambda_1 = \lambda_2 = \mu_0 = \mu_1 = \mu_2 = 0$ at $t = 0$. To obtain average molecular weights from the moments calculated in the model, the following equations are used:

$$\bar{M}_n = (\mu_1 + \lambda_1)/(\mu_0 + \lambda_0) \tag{19}$$

$$\bar{M}_w = (\mu_2 + \lambda_2)/(\mu_1 + \lambda_1) \tag{20}$$

Note that eq 19 and 20 are often approximated by $\bar{M}_n = \mu_1/\mu_0$ and $\bar{M}_w = \mu_2/\mu_1$, where the growing-radical contributions are ignored. The accuracy of this approximation diminishes at high conversions beyond the onset of the autoacceleration region as a result of a large accumulation of growing radicals. Under these circumstances, eq 19 and 20 represent a more realistic description of the system and should be used to deduce the average molecular weights over the entire course of reaction.

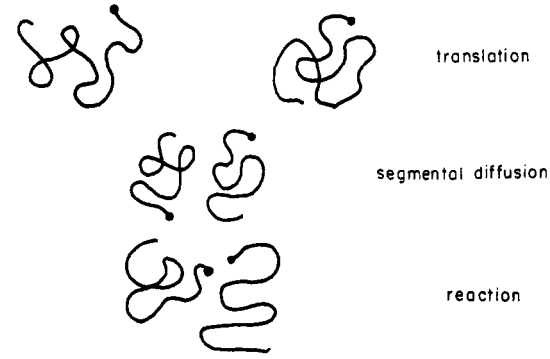

Figure 1. Molecular processes involved in the termination step of free-radical polymerization. Growing radicals are brought together by translational diffusion, whereupon the radical ends reorient by segmental diffusion to facilitate reaction.

2. Constitutive Equations for the Gel and Glass Effects. We now concentrate on establishing a simple algorithm to compute k_t over the entire course of reaction. The termination rate depends on the temperature, chain mobility (thus diffusion), molecular weight of the diffusing species, and composition of the medium. These considerations must all be incorporated into the mathematical description underlying the calculation of k_t. To accomplish this major task, the starting point of modeling requires a careful examination of the fundamental molecular processes involved in chain termination. Figure 1 schematically represents the most prevalent idea concerning the elementary processes constituting termination. Initially, the individual polymer radicals, on average, are located more than a molecular diameter apart. Translational diffusion through a viscous polymer–monomer mixture brings the radical pair closer together, whereupon segmental diffusion orients the chains to facilitate collision of radical ends. Thus, once the molecules migrate to within one molecular diameter, termination reaction follows—but only after the radicals are properly oriented upon conformational rearrangements.

The above description of the sequence of events involved in chain termination is only approximately correct. It is perhaps a good approximation when the concentration is dilute and individual coils can be identified. As conversion increases, the dead coils and chain radicals begin to form entanglements, and translational diffusion and segmental diffusion are both significantly retarded. If the radicals indeed remained unchanged in length for most of the time required for termination, then the well-established scaling concepts[13] in polymer physics could predict the concentration and molecular weight dependence of diffusion. This is not valid, however, since the radical length increases with time via the propagation step. As a consequence, during the lifetime of an average radical, no single mo-

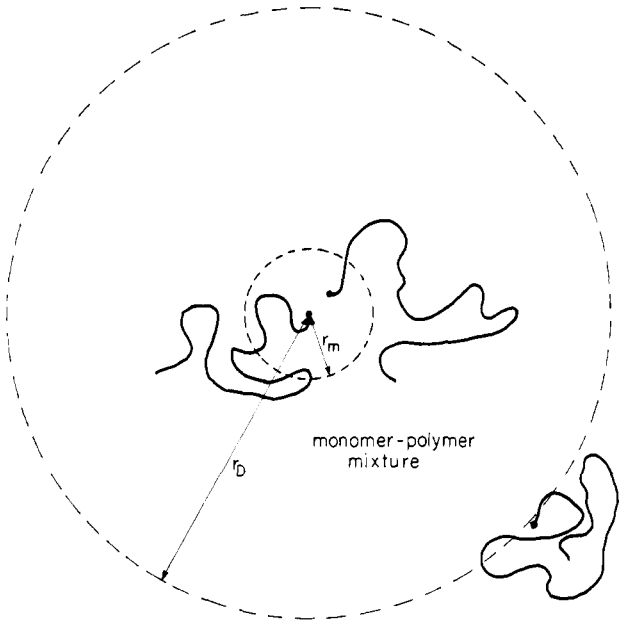

Figure 2. Schematic diagram illustrating the coordinate system used in describing the radical termination process.

lecular weight can realistically represent the radical, making it difficult to apply the scaling concepts. Also, "diffusion" of the radical ends is accomplished not only through diffusion (or reptation for the concentrated case) but also through propagation, which lengthens the radical chain and effectively moves the radical end in spatial position. Hence, migration of the radical ends is achieved via a combined action of diffusion of the entire radical (whose length changes with time) and propagation reaction of the end itself. Since the probability for the end to find a monomer is greater when it propagates outward than inward toward the trailing coil, migration due to propagation may be a significant factor in changes in the radical position with time.

The second difficulty with the conventional modeling approach is associated with the somewhat artificial introduction of a sudden onset of diffusion influence on k_t. In other words, k_t remains constant until either the concentration or some sort of combination of concentration and molecular weight (of the dead polymer) reaches a prescribed critical value, whereupon k_t becomes proportional to the diffusion coefficient. This creates an adjustable parameter to determine when the gel effect computation is switched on—in a somewhat ad hoc fashion. However, diffusion is, in reality, an integral part of the process from the very beginning of polymerization. Its effect on the overall termination rate gradually increases with conversion and becomes dominant around the traditionally so-called "onset point" of the gel effect. A more desirable mathematical form would incorporate both diffusion and reaction limitations from the outset, eliminating the arbitrariness associated with the sudden introduction of the diffusional effect. The relative emphasis of diffusion and reaction may, however, shift with conversion to reflect physical reality.

The approach adopted in the following derivation resembles that used in the classic monograph on the collision theory of chemical reactions in liquids by North.[14] Figure 2 gives an illustrative picture of the termination process with the appropriate coordinate system. We will limit our attention to the radical pair that eventually terminate each other. The distance r_m is the average minimum separation, within which the translational and segmental diffusions necessary for reaction to occur have been completed. This minimum separation can also be viewed as the length scale characterizing the effective sphere swept by the free radical end, similar in concept to the Smoluchowski capture radius.[14] For $r \leq r_m$, the true termination rate constant, k_t^0, characterizes the ensuing collision process. This true rate constant is an intrinsic kinetic parameter, reflecting the rate of reaction under the hypothetical condition unencumbered by diffusion limitations. At a large distance from the radical at the origin, $r \geq r_D$, the concentration of radicals approaches the unperturbed bulk concentration, C_b. The effective concentration, C_m, for $r \leq r_m$ is a function of the radical diffusivity and rate of radical consumption. The overall rate of radical diffusion into the reaction zone bounded by r_m equals the overall rate of radical termination. The migration of the second radical from $r \gg r_m$ to r_m takes place through diffusion and propagation, as discussed earlier. Both can be treated as random walk processes. The random walk statistics can be succinctly transformed into the following mathematical statement for the region between r_m and r_D:[15]

$$4\pi r^2 D \frac{dc}{dr} = K \tag{21}$$

with boundary conditions

$$C = C_m, \quad \text{at } r = r_m$$
$$C = C_b, \quad \text{at } r = r_D$$

In eq 21, D represents the effective migration coefficient resulting from both diffusive and propagational motion. Since $r_D \gg r_m$, eq 21 can be easily integrated to give

$$4\pi D r_m (C_b - C_m) = K \tag{22}$$

The constant, K, is determined by mass balance; i.e., the rate of radical transport into all spherical regions confined by r_m is equal to the rate of radical consumption in the spheres due to termination:

$$4\pi D r_m (C_b - C_m) = \tfrac{4}{3}\pi r_m^3 k_t^0 C_m C_b \tag{23}$$

The right-hand side of this equation gives a second-order rate expression that depends on the probability of finding a radical within distance r_m of a second central radical, C_m, and the probability of finding the central radical in the system, C_b. Equation 23 can be rearranged to give

$$C_m = \frac{DC_b}{D + (r_m^2/3)k_t^0 C_b} \tag{24}$$

Hence, C_m is dictated by both k_t^0 and D. The overall reaction rate is ordinarily expressed as $k_t C_b^2$, where k_t is the apparent rate constant. This rate is the same as $k_t^0 C_m C_b$, so that we have

$$k_t C_b^2 \equiv k_t^0 C_m C_b \tag{25}$$

Equations 24 and 25 yield the following result:

$$\frac{1}{k_t} = \frac{1}{k_t^0} + \frac{r_m^2 C_b}{3D} \tag{26}$$

This final result in essence attributes the overall resistance encountered in chain termination to the sum of both a reaction-limited and mass-transfer-limited term.

We will assume that r_m is relatively insensitive to temperature, concentration, and radical molecular weight to facilitate subsequent discussions. Both k_t^0 and D acquire strong temperature dependence in view of the fact that they represent activated processes. The former lacks concentration and molecular weight dependence, by our definition, whereas the latter assumes strong dependence

on both concentration and molecular weight. Separating D into a temperature- and molecular-weight-dependent front factor, D_0, and a conversion-dependent part, $f(x)$, we have

$$\frac{1}{k_t} = \frac{1}{k_t^0} + \frac{r_m^2}{3D_0}\frac{C_b}{f(x)} \equiv \frac{1}{k_t^0} + \theta_t\frac{C_b}{f(x)} = \frac{1}{k_t^0} + \theta_t\frac{P}{f(x)} \quad (27)$$

where $\theta_t \equiv r_m^2/3D_0$ has dimensions of time and can be viewed as a characteristic migration time of the growing radicals.

For the glass effect occurring only at very high conversions, even diffusion of monomers in the now extremely viscous medium is impeded. This process is amenable to similar mathematical treatment, i.e., fixing the radical end at the coordinate origin and analyzing the diffusion-limited propagation reaction by calculating the effective concentration of the monomer in the vicinity of the growing radical. An analogous derivation gives the following equation, relating the apparent k_p with the true k_p^0:

$$\frac{1}{k_p} = \frac{1}{k_p^0} + \theta_p\frac{P}{g(x)} \quad (28)$$

where θ_p is the characteristic monomer diffusion time, which is only a function of temperature but not of molecular weight of the polymer, and $g(x)$ accommodates the conversion dependence of monomer diffusion due to the increasing viscosity of the medium. Equations 27 and 28 are then used in conjunction with eq 10–18 for model simulation.

The major task remaining is to establish the temperature and molecular weight dependence of θ_t, the temperature dependence of θ_p, and the forms of $f(x)$ and $g(x)$. To this end, we invoke the Fujita–Doolittle theory based on the free volume concept:[16,17]

$$\log\frac{D}{D_0} = \frac{\phi_m}{A(T) + B(T)\phi_m} \quad (29)$$

where ϕ_m is the volume fraction of the monomer, A and B are functions of temperature, and D_0 is the diffusion coefficient at the limit of vanishing ϕ_m. As mentioned previously, mass transfer of the radical end is achieved via the combined action of chain growth and diffusion. Also, the radical end is often attached to a long-chain molecule. Both considerations would initially suggest that eq 29 may not apply directly to the situation of gel effect. However, chain growth involves addition of monomers to the radical end; its rate is dictated by the mobility of monomers (thus eq 29 applies). Furthermore, even translational motion of the whole chain represents merely a concerted sequence of events involving segmental hopping. It, too, is subjected to the concentration dependence given by eq 27. Finally, segmental diffusion definitely follows eq 29, since the hopping units are comparable in size to a monomer. These considerations support the use of eq 29 for the concentration dependence of diffusivity. Dependence on chain length of the migrating radicals is best accommodated in D_0. However, because of the complicated nature of the radical termination process (recall that the chain length increases during diffusion), this molecular weight dependence cannot possibly take on any simple form, e.g., a power relationship as described by the scaling laws. Since the molecular weights of both the polymer radical and the dead polymer are functions of the initiator loading, we will assume that $D_0 = D_0(I_0)$. The result is that $\theta_t = \theta_t(I_0)$. The exact functional dependence must be determined by fitting experimental data and will be investigated further in a later section. For monomer diffusion in the glass effect region, eq 29 can be used exactly. However, D_0 does not have any molecular weight dependence, since only monomer diffusion is involved. This allows only temperature dependence in θ_p. In eq 29, the volume fraction of the monomer, ϕ_m, is related to conversion by

$$\phi_m = \frac{(1-x)/d_m}{x/d_p + (1-x)/d_m} = \frac{1-x}{1+\epsilon x} \quad (30)$$

Substitution of eq 29 and 30 into eq 27 and 28 gives the following final forms for the constitutive equations used in this model:

$$\frac{1}{k_t} = \frac{1}{k_t^0(T)} + \theta_t(T,I_0)\frac{P}{\exp\left[\dfrac{2.3\phi_m}{A(T) + B(T)\phi_m}\right]} \quad (31)$$

and

$$\frac{1}{k_p} = \frac{1}{k_p^0(T)} + \theta_p(T)\frac{P}{\exp\left[\dfrac{2.3\phi_m}{A(T) + B(T)\phi_m}\right]} \quad (32)$$

A list of numerical values (e.g., the reaction rate constants) used in the calculation is given in Table I. We will discuss the remaining four model parameters, θ_t, θ_p, A, and B, in detail in the next section. Note that termination by recombination is ignored in the calculation, so the molecular weight predictions will be underestimated.

Table I
Numerical Values of Parameters Used in Model Calculation[6,7]

$f = 0.58$
k_d (L/min) = $6.32 \times 10^{16} \exp[-15.43 \times 10^3/T\,(\mathrm{K})]$
k_t^0 (L/(min-mol)) = $5.88 \times 10^9 \exp[-701/1.987T\,(\mathrm{K})]$
k_p^0 (L/(min-mol)) = $2.95 \times 10^7 \exp[-4353/1.987T\,(\mathrm{K})]$
$k_{tc} = 0$ [termination by disproportionation only]
d_p (g/cm³) = 1.2
d_m (g/cm³) = $0.973 - 1.164 \times 10^{-3}(T\,(\mathrm{K}) - 273)$
T_{gp} (°C) = 114

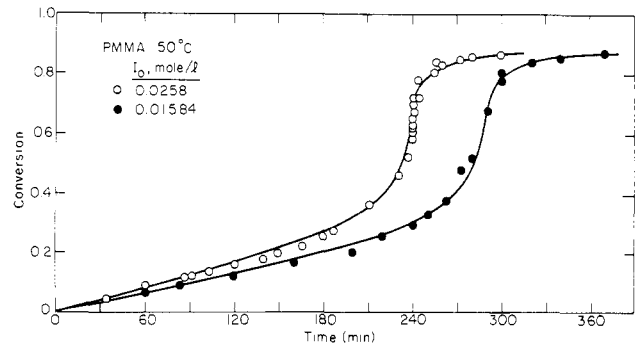

Figure 3. Conversion histories of PMMA polymerization at 50 °C with two initiator loadings. Circles are experimental data[7] and solid curves are computed by the model.

Results and Discussion

In this section, model predictions are compared with literature data on conversion history and evolution of average molecular weights for poly(methyl methacrylate) (PMMA) polymerization conducted isothermally at different controlled temperatures.

Figures 3–9 give the comparison of calculated curves with literature data on PMMA at 50, 70, and 90 °C.[7] Two initiator loadings were used in the experiments, leading to quite different conversion histories at the same temperature. The model successfully predicts the conver-

Table II
Model Parameters Used in Fitting Experimental Data

polym temp, °C	initiator loading, mol/L	θ_t, min	θ_p, min	A	B
50	0.0258	1.50×10^3	3.5×10^3	0.134	0.03
	0.01548	2.33×10^3	3.5×10^3	0.134	0.03
70	0.0258	4.90×10	2.5×10^2	0.152	0.03
	0.01548	8.30×10	2.5×10^2	0.152	0.03
90	0.0258	3.80	3.0×10	0.163	0.03
	0.01548	6.30	3.0×10	0.163	0.03

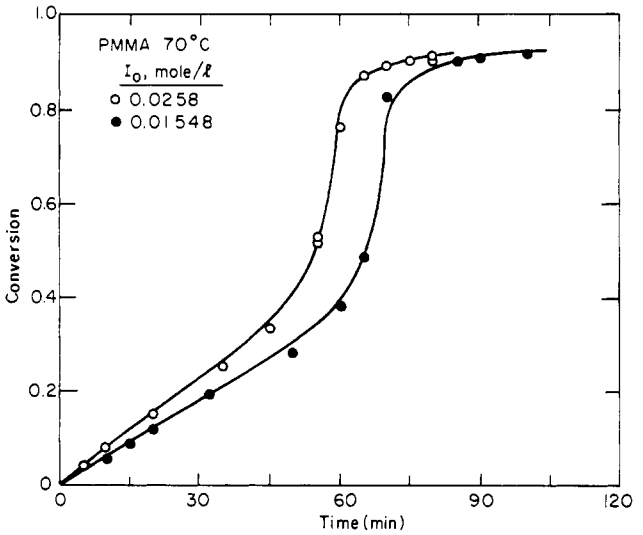

Figure 4. Conversion histories of PMMA polymerization at 70 °C with two initiator loadings. Circles are experimental data[7] and solid curves are computed by the model.

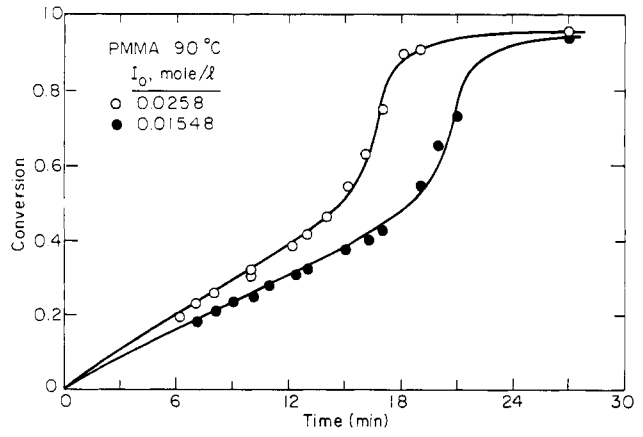

Figure 5. Conversion histories of PMMA polymerization at 90 °C with two initiator loadings. Circles are experimental data[7] and solid curves are computed by the model.

sion–time plots for different temperatures and initiator concentrations. Table II summarizes the model parameters used for the experimental conditions examined. Note that the limiting conversion at long times is lowest at 50 °C and gradually increases with the polymerization temperature. This is consistent with the glass effect, whereby the reaction mixture essentially freezes at a composition whose T_g corresponds to the reaction temperature. Another important feature characterizing both the experimental data and the predicted curves is the curvature of the conversion history before the onset of the so-called gel region. Note that these curves are concave upward preceding the sharp rise. If the gel effect were suddenly switched on at a certain critical conversion level, the portion of the conversion curve under examination would be concave downward due to the gradual depletion of

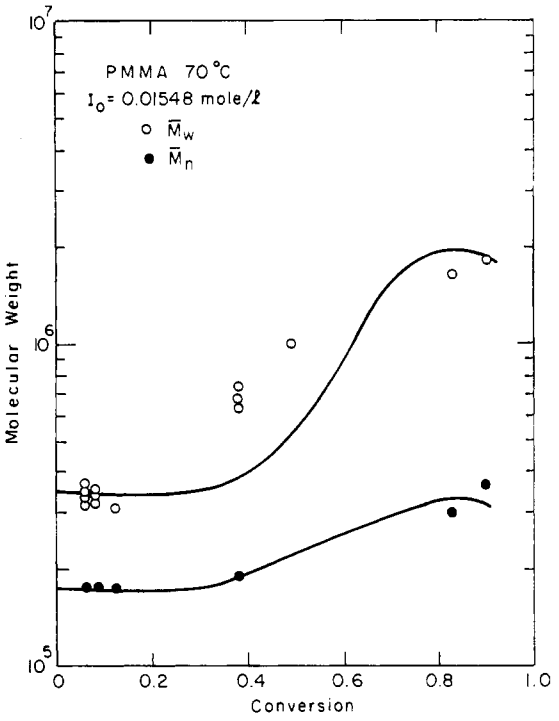

Figure 6. Average molecular weights as functions of conversion for PMMA polymerization at 70 °C and initiator loading of 0.01548 mol/L. The circles represent experimental data[7] and the solid curves are predicted by the model.

monomer. Beyond this critical conversion, the gel effect algorithm is suddenly switched on in the model, causing a discontinuous slope in the conversion curve. Hence, a major difference exists between the present model and other contemporary ones in that this model incorporates diffusion in the basic sequence of events constituting the termination of growing radicals from the very outset of reaction. Onset of gel effect is only a convenient phrase denoting the region of rapid rise in the conversion. There exists in fact no sharp demarcation in terms of molecular processes before and after the "occurrence" of this autoacceleration region. The rapid rise in conversion is merely a natural consequence of the increasing importance of mass transfer limitations. The approach adopted here eliminates the need to introduce a critical parameter to separate the conversion history into mathematically different regions.

The average molecular weights computed by this model compare favorably with the experimental results[7] as shown in Figures 6–9. Discrepancies, however, can be seen around the region of rapid polymerization. These are more pronounced for $\bar{M}_w$ than $\bar{M}_n$. This weakness is shared by many other models,[5,7,8] and its cause is unknown at present. The presence model, however, successfully correlates $\bar{M}_w$ and $\bar{M}_n$ at various conversion levels with temperature and initiator loading. Note that at the same temperature, a higher initiator concentration results in a lower molecular

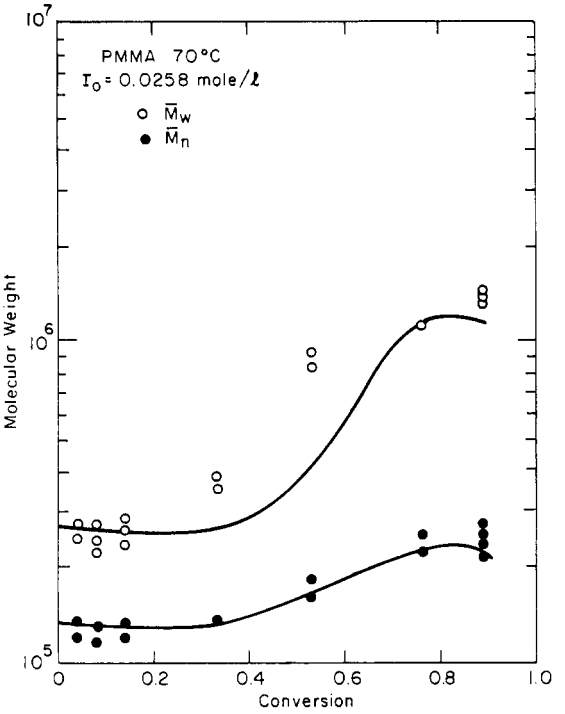

Figure 7. Average molecular weights as functions of conversion for PMMA polymerization at 70 °C and initiator loading of 0.0258 mol/L. The circles represent experimental data[7] and the solid curves are predicted by the model.

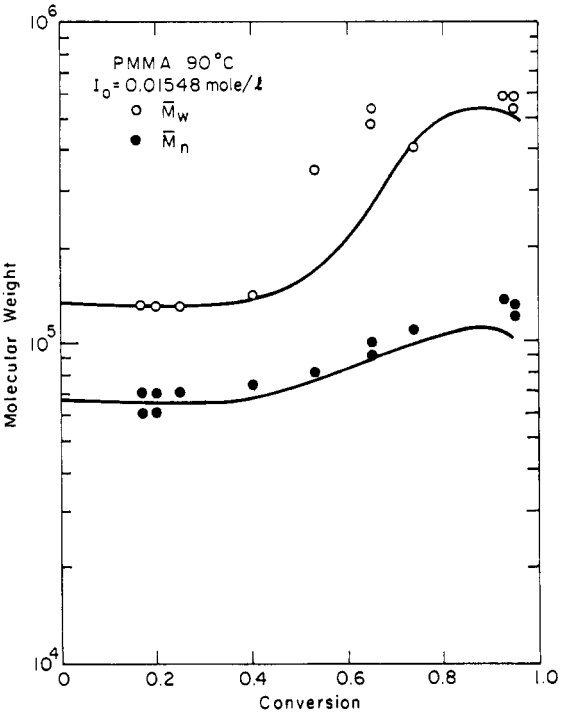

Figure 8. Average molecular weights as functions of conversion for PMMA polymerization at 90 °C and initiator loading of 0.01548 mol/L. The circles represent experimental data[7] and the solid curves are predicted by the model.

weight. Also, increasing temperature at a constant initiator loading significantly lowers the molecular weight. At high conversions, when termination rate is greatly reduced, the average molecular weights rise appreciably.

The calculated k_t and k_p as functions of conversion at the three temperatures studied are shown in Figures 10–12. Both exhibit an initial plateau at low conversions and decrease monotonically with conversion. Termination becomes significantly affected at a much lower conversion

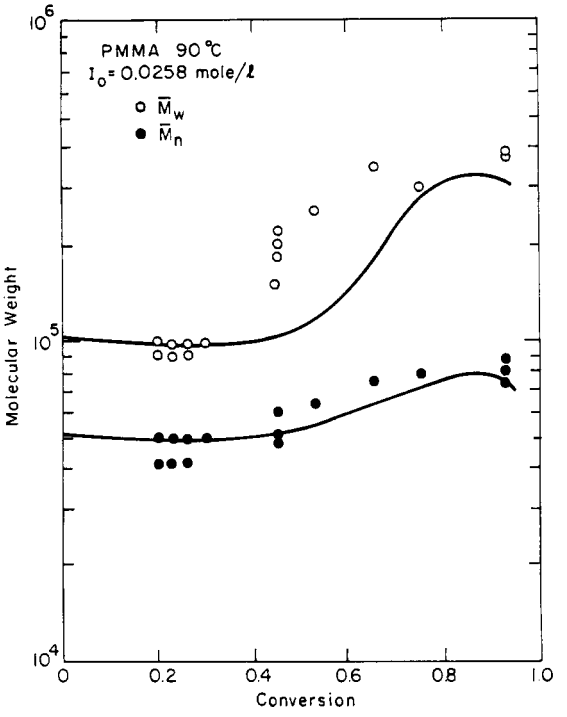

Figure 9. Average molecular weights as functions of conversion for PMMA polymerization at 90 °C and initiator loading of 0.0258 mol/L. The circles represent experimental data[7] and the solid curves are predicted by the model.

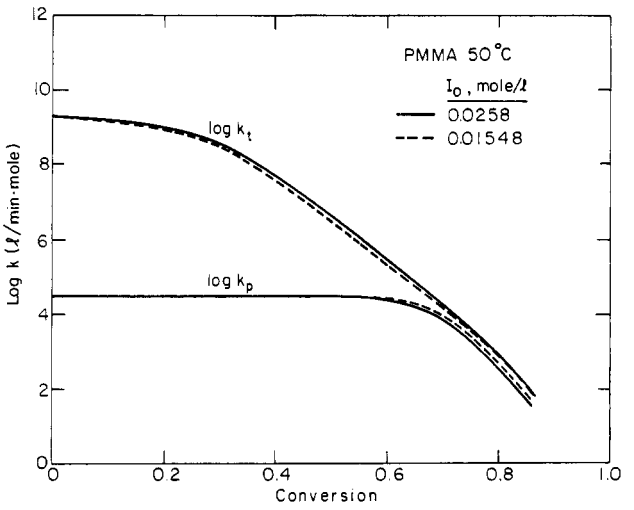

Figure 10. Calculated apparent termination and propagation rate constants as functions of conversion for polymerization at 50 °C.

level than propagation. The "bend" of the log k_t curve determined by extrapolating the sloped region to intersect with the initial value gives a qualitative impression of the "onset" of gel effect. This intersection occurs around a conversion level of 0.26 for 50 °C, 0.35 for 70 °C, and 0.45 for 90 °C. This trend indicates that diffusion limitation is most marked at low temperatures; its influence becomes significant at lower conversion levels. Similarly, the drop-off in k_p is delayed by increasing temperature. Note also that initiator loading has very little effect on both curves.

We next investigate the dependence of model parameters on the various operating variables of the polymerization process, i.e., I_0 and T. Figure 13 plots the natural logarithm of both $1/\theta_t$ and $1/\theta_p$ vs. $1/T$. According to eq 27 and 28, the temperature dependence of $1/\theta_t$ and $1/\theta_p$ reflects primarily the behavior of D_0 for termination and

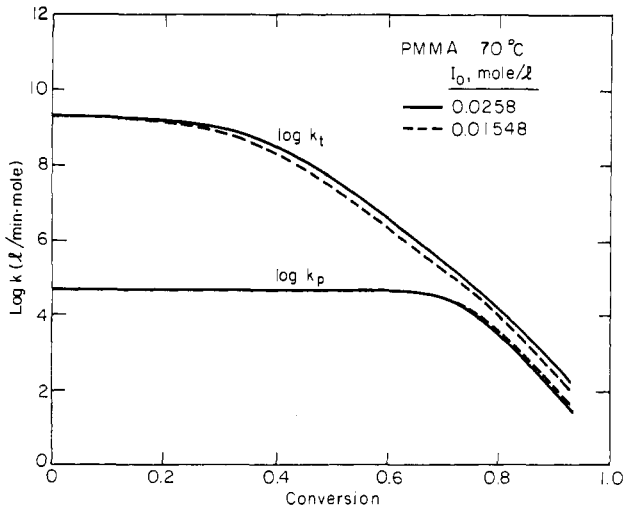

Figure 11. Calculated apparent termination and propagation rate constants as functions of conversion for polymerization at 70 °C.

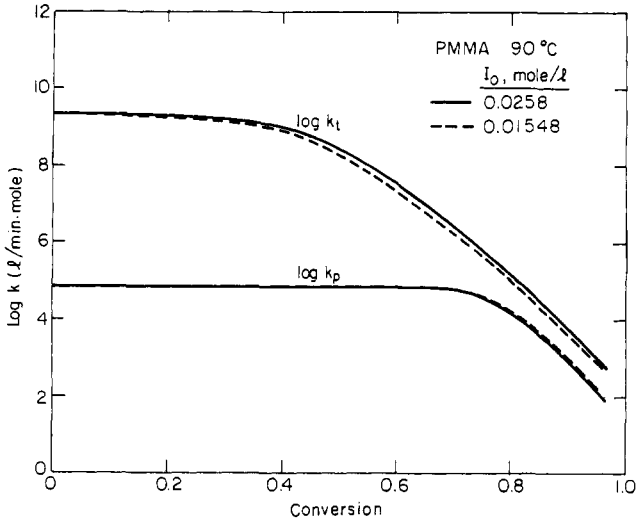

Figure 12. Calculated apparent termination and propagation rate constants as functions of conversion for polymerization at 90 °C.

propagation, respectively. Since D_0 apparently exhibits an Arrhenius temperature dependence, the slope of the curves in Figure 13 leads to the activation energy of the mass transport processes for growing radicals and monomers. The former has an activation energy of 34 kcal/mol, whereas the latter gives 28 kcal/mol. Note that θ_t is consistently greater at the lower initiator loading, presumably due to a weak dependence of D_0 on molecular weight (as the lower I_0 results in a higher molecular weight, which decreases D_0).

The remaining two parameters in the model, $A(T)$ and $B(T)$ in eq 29, are examined in Figure 14. It has been found empirically that $B(T)$ is not sensitive to temperature for many systems[16] and can be treated as a constant. We have taken B to be 0.03 throughout this work, which yields successful predictions. The values of A chosen for data fitting are plotted against T. In general, A increases with T. However, since there are only three points on the curve, it is difficult to use the existing information for accurate interpolation and extrapolation to estimate A at other temperatures. This is remedied by noting that A scales linearly with $(T - T_{gp})^2$, where T_{gp} is the glass transition temperature of the pure polymer. Indeed, the values of A used in the model calculation obey this relation as shown in Figure 15. Figures 13 and 15 provide an effective means

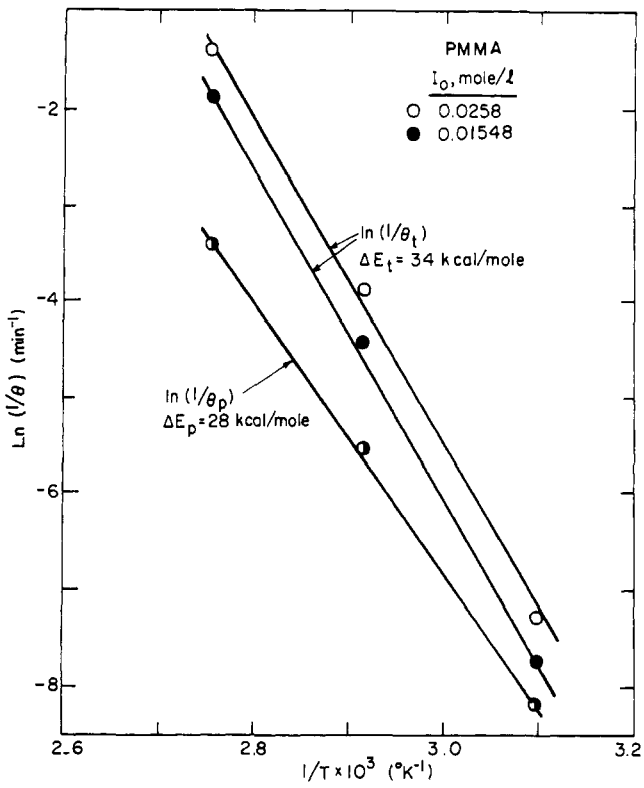

Figure 13. Model parameters θ_t and θ_p chosen for the best fit of experimental data.[7] The Arrhenius plots give activation energies of 34 and 28 kcal/mol for the mass transfer processes in termination and propagation, respectively.

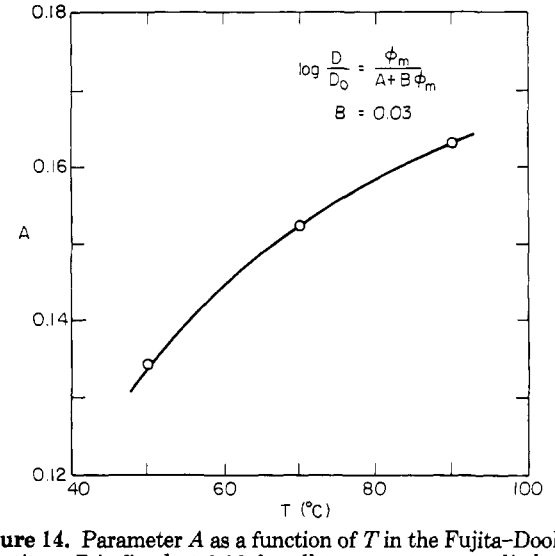

Figure 14. Parameter A as a function of T in the Fujita–Doolittle equation. B is fixed at 0.03 for all temperatures studied.

to estimate all the model parameters for model predictions corresponding to polymerization over a wide temperature range.

Finally, we investigate the errors introduced by the quasi-steady-state assumption (QSSA) on the growing-radical population. Up to now, all predictions were made by solving the set of simultaneous ordinary differential equations outlined previously. The use of QSSA eliminates three, i.e., eq 12–14, and replaces them by three algebraic equations obtained by equating the left-hand side of eq 12–14 to zero. Solutions of this new set of differential and algebraic equations are given in Figures 16–18. Figure 16 shows that the radical concentrations calculated using either the exact solution or the QSSA are essentially

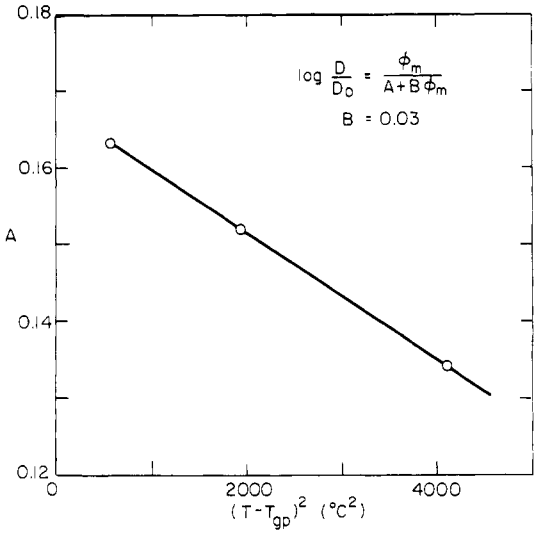

Figure 15. Parameter A in the Fujita–Doolittle equation plotted vs. $(T - T_{gp})^2$, where T_{gp} is the glass transition temperature of the bulk PMMA. All three points fall on the same straight line, facilitating interpolation and extrapolation to estimate A at other polymerization temperatures.

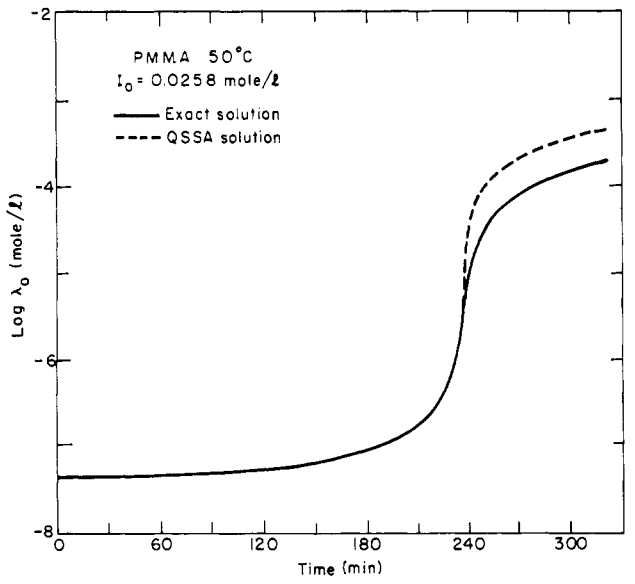

Figure 16. Radical concentration as a function of time computed for the condition of 50 °C and initiator loading of 0.0258 mol/L. The solid curve represents the exact solution; the dashed one is the QSSA result. Note the rapid buildup of the radical population in the gel effect region.

identical prior to the region of rapid conversion. Beyond this region, the predicted radical concentrations differ significantly. The QSSA solution overestimates the radical concentration by more than a factor of 2. Given such a large discrepancy, the conversion–time curves calculated by the exact and approximate solution are surprisingly consistent (Figure 17). The agreement extends well into the glass effect region. This is because the discrepancy in the radical concentration in Figure 16 occurs only in a region where the rate of polymerization has slowed down sufficiently; i.e., the rate is no longer governed by the radical population but by the diffusion limitation of monomers to the reactive sites. The use of approximate solution does indeed have a noticeable effect on the predicted molecular weights as shown in Figure 18. However, if only the ultimate $\bar{M}_w$ is desired, QSSA gives results almost identical with the exact solution. This agreement may be fortuitous, as $\bar{M}_n$ predictions differ even in the neighborhood of limiting conversion.

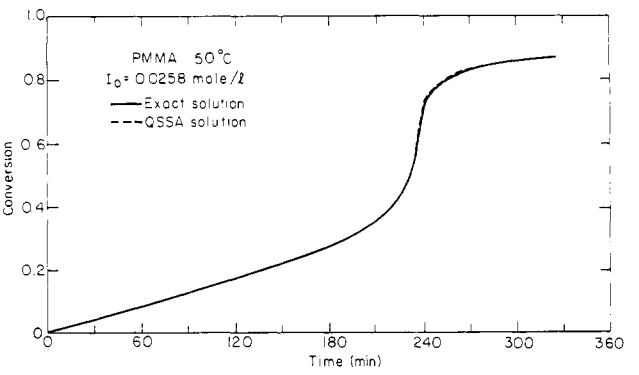

Figure 17. Conversion histories calculated using the exact (solid curve) and QSSA (dashed curve) method.

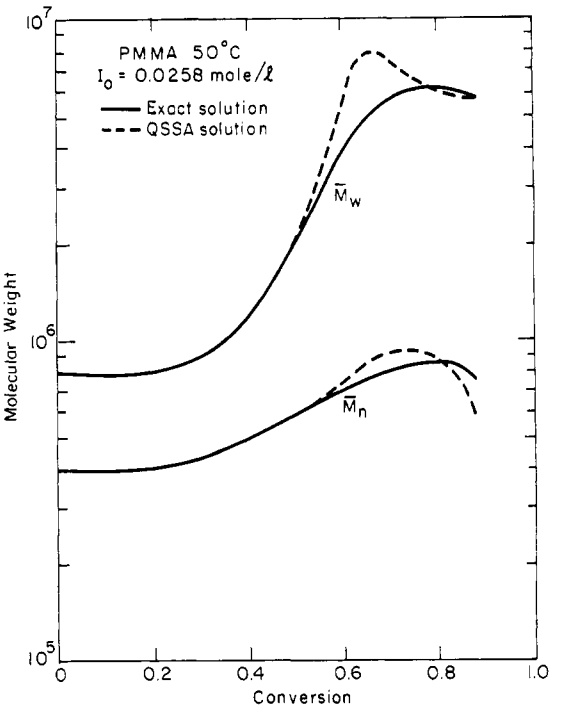

Figure 18. Average molecular weights calculated using the exact (solid curve) and QSSA (dashed curve) method.

In conclusion, we have developed a molecular model for the description and prediction of free-radical chain polymerization processes. This model incorporates considerations of mass transfer from the beginning of the reaction. Hence, it does not require artificially imposed break points for the introduction of diffusion limitation to the termination and propagation steps. One unified equation applies to the evaluation of k_t and k_p over the entire course of reaction. Finally, model parameters are linked to the operating variables of the process, in particular, to the prevailing temperature of the system. This allows for ready extension of the model to predictions of conversion and molecular weights, given a known temperature history. Results of nonisothermal experiments with known temperature histories will be highly useful in the further scrutiny of the present model.

Acknowledgment. This work was supported by National Science Foundation Initiation Grant CPE 8103632.

Registry No. Methyl methacrylate, 80-62-6.

References and Notes

(1) Trommsdorff, V. E.; Kohle, H.; Lagally, P. *Makromol. Chem.* **1947**, *1*, 169.
(2) Schulz, G. V.; Harborth, G. *Makromol. Chem.* **1947**, *1*, 106.

(3) Cardenas, J. N.; O'Driscoll, K. F. *J. Polym. Sci., Polym. Chem. Ed.* **1976**, *14*, 883.
(4) Arai, K.; Saito, S. *J. Chem. Eng. Jpn.* **1976**, *9*, 302.
(5) Ross, R. T.; Laurence, R. L. *AIChE Symp. Ser.* **1976**, *No. 160*, 74.
(6) Schmidt, A. D.; Ray, W. H. *Chem. Eng. Sci.* **1981**, *36*, 1401.
(7) Marten, F. L.; Hamielec, A. E. *ACS Symp. Ser.* **1979**, *No. 104*, 43.
(8) Tulig, T. J.; Tirrell, M. *Macromolecules* **1981**, *14*, 1501.
(9) Benson, S. W.; North, A. M. *J. Am. Chem. Soc.* **1959**, *81*, 1339.
(10) North, A. M.; Reed, G. A. *Trans. Faraday Soc.* **1961**, *57*, 859.
(11) Brooks, B. W. *Proc. R. Soc. London, Ser. A* **1977**, *357*, 183.
(12) High, K. A.; Lee, H. B.; Turner, D. T. *Macromolecules* **1979**, *12*, 332.
(13) de Gennes, P.-G. "Scaling Concepts in Polymer Physics"; Cornell University Press: Ithaca, NY, 1979.
(14) North, A. M. "The Collision Theory of Chemical Reactions in Liquids"; Wiley: New York, 1964.
(15) Bird, R. B.; Armstrong, R. C.; Hassager, O. "Dynamics of Polymeric Liquids"; Wiley: New York, 1977; Vol. I, p 71.
(16) Fujita, H.; Kishimoto, A.; Matsumoto, K. *Trans. Faraday Soc.* **1960**, *56*, 424.
(17) Middleman, S. "Fundamentals of Polymer Processing"; McGraw-Hill: New York, 1977; p 362.

Radical Reactions of Highly Polar Molecules. Hydrocarbons as Chain-Transfer Agents in Fluoro Olefin Telomerizations†

Leonard O. Moore

Weslaco Technical Center, The Ansul Company, Weslaco, Texas 78596.
Received December 2, 1981

ABSTRACT: Hydrocarbons act as chain-transfer agents to provide telomeric products in the radical polymerization of tetrafluoroethylene. At 125 °C, linear alkanes (hexane, nonane, and decane) participate by transferring more than one hydrogen; by contrast, cyclopentane and cyclohexane do not. Methylcyclohexane is attacked only at the tertiary hydrogen. For comparison, the chain transfer of nonane with hexafluoropropene and chlorotrifluoroethylene as well as with tetrafluoroethylene was studied.

Although there is considerable literature on the abstraction of hydrogens by halogen atoms[1-4] and various other radicals,[5] there is little information on the reactivity of hydrocarbons as chain-transfer agents,[6] particularly for fluorinated olefins. In earlier papers we described the relative reactivities of halogenated olefins,[7] the chloromethanes,[8] and several other halocarbons[9] with tetrafluoroethylene and the use of chain-transfer constants to correlate reactivity on radical abstraction reactions to bond energy.

We have now examined the reactivity of a few hydrocarbons as chain-transfer agents in telomerization with tetrafluoroethylene and also compared the reactivity of nonane with telomer chains of tetrafluoroethylene, hexafluoropropene, and chlorotrifluoroethylene.

Experimental Section

Reaction of Hexane with Tetrafluoroethylene. A mixture of 20 g of hexane, 1.6 g of benzoyl peroxide, and 60 g of 1,1,2-trichloro-1,2,2-trifluoroethane was charged to a 300-cm^3 autoclave.[10] The autoclave was closed, cooled in a dry ice–acetone bath, and evacuated to below 50 mm, and 20 g of tetrafluoroethylene[11] was added. More than the desired 20 g of tetrafluoroethylene was charged, so the excess was bled off after the autoclave had warmed slightly. The mixture was stirred and heated. It required 1 h to reach 125 °C, where it was held for an additional hour. After the mixture cooled, unreacted tetrafluoroethylene was bled into a dry ice–acetone-cooled trap and the remaining material was distilled to separate unreacted hexane and fluorocarbon solvent. The residue was a waxy solid, mp 27–32 °C.

Elemental analyses of carbon and fluorine were used to calculate the average molecular weight and average degree of telomerization $\bar{n}$. The values agree within about 2%.

$$\bar{n} = [\%\ C \times (\text{mol wt of telogen}) - 1201.1 \times (\text{no. of C in telogen})]/[2402.2 - \%\ C \times (\text{mol wt of } C_2F_4)]$$

$$\bar{n} = [\%\ F \times (\text{mol wt of telogen})]/[4 \times 18.998 \times 100 - \%\ F \times (\text{mol wt of } C_2F_4)]$$

mol wt of telomer = (mol wt of telogen) + $\bar{n}$ × (mol wt of C_2F_4)

The concentrations of reactants in the liquid phase were estimated by noting the total pressure and estimating partial pressures of telogen and solvent based on the vapor pressures and relative concentrations. The difference of pressure was assumed to be due to tetrafluoroethylene.

$$P_{C_2F_4} = P_{total} - (P_{telogen} + P_{solvent})$$

The amount of tetrafluoroethylene in the vapor phase was then estimated by the gas equation, where the volume was that volume above the liquid phase. From this the concentration of tetrafluoroethylene in the liquid phase could be calculated.

$$C_2F_{4\,soln} = C_2F_{4\,total} - C_2F_{4\,vapor}$$

The chain-transfer constant was calculated by the method of Walling.[12]

$$C = \frac{1}{\bar{n}} \frac{[C_2F_4]}{[\text{telogen}]}$$

NMR spectra of the telomer residues were obtained with a Varian HA-100 spectrometer to indicate the extent of branching and, where possible, the position of attack.

Since in the linear alkanes there was more than one telomer chain initiated per molecule of hydrocarbon, a second chain-transfer constant was calculated as $\bar{n}' = \bar{n}/(\text{no. of branches})$. This is designated as C' in Table I and is used for comparisons in the Discussion.

The results of the experiments are presented in Table I and the NMR results are presented in the Discussion.

Discussion

Normal Alkanes. The reactivity to hydrogen abstraction by fluoroalkyl radicals increases with increasing chain length of the normal alkanes as noted in Table I. The reactivity is on a molar basis because the primary and secondary hydrogens were not sufficiently resolved in the NMR spectra. Thus the reactivities of these two types of hydrogen could not be distinguished. The reactivity is compared on the basis of the number of telomer chains formed. The normal alkanes did not give only one fluo-

† Work done at Union Carbide Corp.

0024-9297/83/2216-0357$01.50/0